In-Depth Activation of Channelrhodopsin 2-Sensitized Excitable Cells with High Spatial Resolution Using Two-Photon Excitation with a Near-Infrared Laser Microbeam

Samarendra K. Mohanty,* Rainer K. Reinscheid,[†‡§] Xiaobin Liu,[†‡] Naoe Okamura,[‡] Tatiana B. Krasieva,* and Michael W. Berns*

*Beckman Laser Institute, [†]Department of Pharmaceutical Sciences, [‡]Department of Pharmacology, and [§]Department of Molecular Biology and Biochemistry, University of California, Irvine, California

ABSTRACT We used two-photon excitation with a near-infrared (NIR) laser microbeam to investigate activation of channelrhodopsin 2 (ChR2) in excitable cells for the first time to our knowledge. By measuring the fluorescence intensity of the calcium (Ca) indicator dye, Ca orange, at different wavelengths as a function of power of the two-photon excitation microbeam, we determined the activation potential of the NIR microbeam as a function of wavelength. The two-photon activation spectrum is found to match measurements carried out with single-photon activation. However, two-photon activation is found to increase in a nonlinear manner with the power density of the two-photon laser microbeam. This approach allowed us to activate different regions of ChR2-sensitized excitable cells with high spatial resolution. Further, in-depth activation of ChR2 in a spheroid cellular model as well as in mouse brain slices was demonstrated by the use of the two-photon NIR microbeam, which was not possible using single-photon activation. This all-optical method of identification, activation, and detection of ChR2-induced cellular activation in genetically targeted cells with high spatial and temporal resolution will provide a new method of performing minimally invasive in-depth activation of specific target areas of tissues or organisms that have been rendered photosensitive by genetic targeting of ChR2 or similar photo-excitable molecules.

INTRODUCTION

Considerable efforts have been made to control neuronal growth and activities using near-infrared (NIR) light (1–3). Recently, visible light-assisted activation of selected groups (expressing the same gene) of electrically excitable cells, such as neurons, with high temporal precision (4) was made possible by the introduction of a light-activated molecular channel (5), channelrhodopsin-2 (ChR2), into specific groups of cells. This eliminates the highly challenging requirement of placing electrodes inside every single neuron of a chemically identified group of cells. This method also has several advantages over electrical stimulation, such as cellular specificity and noninvasiveness. Since ChR2 is a nonselective cation channel, light-induced activation of ChR2 results in depolarization of only those neurons that express ChR2. Selective activation of neurons by ms-pulsed blue light has been demonstrated in cell culture (6), brain slices (7), and small animals (8,9). This method requires light of very low intensity (a few mW/mm^2) that can be delivered from a lamp with a bandpass filter or small laser diode. However, since the activation peak of ChR2 is ~460 nm, where absorption and scattering coefficients of biological tissue are very high, penetration of the activating light beam is very much limited. One approach to overcome this limitation would be to modify the activation spectrum of ChR2, which can enable excitation of cells at longer wavelengths. However, this might not be as straightforward (10) as the evolution of ubiquitous green-fluorescent protein (GFP) and its variants, since ChR2 requires retinal as the chromophore rather than a fluorophore formed by the protein itself, as in GFPs. Further, some experiments may necessitate selective activation of single cells or even different locations in the same cell. Since the single-photon (blue) light beam cannot be spatially confined to a very small volume, it is difficult to activate subregions of ChR2-expressing cells without affecting the neighboring microscopic regions.

Two-photon scanning laser microbeams have revolutionized the field of functional biological imaging (11) and manipulation (12,13). The focal point specificity of the technique provides the capability to image objects at the focal plane with little or no collateral excitation and can be used to selectively inactivate genes (13), and reduced scattering cross section and absorption in the tissue ''optical window'' at 700–1000 nm provides deeper penetration. Indeed, single-photon activation of ChR2 was recently coupled with two-photon calcium (Ca) imaging for visualization of activation processes in cells (14). However, two-photon activation of ChR2 has not yet been reported, to our knowledge. Here we report the use of NIR two-photon absorption to activate genetically targeted excitable cells at significantly greater depths (as compared to single-photon absorption) and with high spatial resolution. These results will enable in vivo applications of the ChR2 technology with better optical identification, activation, and imaging efficacy.

Submitted January 28, 2008, and accepted for publication May 28, 2008.

Address reprint requests to Samarendra K. Mohanty, E-mail: smohanty@uci.edu.

Editor: Francisco Bezanilla.

0006-3495/08/10/3916/11 $2.00

doi: 10.1529/biophysj.108.130187

MATERIALS AND METHODS

Cell culture

HEK 293 cells were transfected with the ChR2 enhanced yellow fluorescent protein (EYFP) construct, cloned into pcDNA3.1 neo (Invitrogen). ChR2 cDNA was kindly provided by Dr. Georg Nagel (University of Wuerzburg, Wuerzburg, Germany). EYFP was fused in-frame to the C-terminus of ChR2 by polymerase chain reaction (PCR). Transgene-expressing cells were identified by visualizing the EYFP fluorescence under suitable illumination (514 nm). Stable clones were selected with 200 mg/L G418 and colonies were picked after 2 weeks and then expanded. Clones that showed the highest level of EYFP fluorescence were chosen for the optical activation experiments. For optical detection of the activation process, cells were incubated with 1 μM Ca orange (Invitrogen, Carlsbad, CA) for 10 min and washed thereafter. Cells were maintained at 37°C, 5% CO_2 in Dulbecco's modified Eagle's medium containing 10% fetal bovine serum.

Hippocampal tissue slice preparation

A cDNA construct encoding ChR2 with a C-terminally fused EYFP reporter was cloned into the lentiviral expression vector pLenti6/R4R2/V5-DEST that carries no promoter (Invitrogen). At the 5′-end of this construct, a CMV promoter sequence was inserted. Recombinant viruses were produced according to the manufacturer's protocol. A dose of 5×10^6 viral particles in a total volume of 1 μL was injected into the CA3 area of the hippocampus of C57Bl/6 mice that had been anesthetized with ketamine/xylazine. One week later, the animals were killed and their brains were extracted and embedded in 2% low melting agarose. Brain slices (300 μm) were prepared using a vibratome in an ice-cold solution that contained (in mM): 125 NaCl, 2.5 KCl, 2 $CaCl_2$, 1 $MgCl_2$, 1.25 NaH_2PO_4, 26 $NaHCO_3$, and 25 D-glucose, bubbled with oxycarbon (95% O_2/5% CO_2), pH 7.4, and were subsequently incubated at 20°C in the same solution. Slices were inspected for expression of EYFP under illumination at 488 nm. Slices containing hippocampal areas were incubated with 5 μM Ca orange for 20 min and washed thereafter. All animal experiments were approved by the local institutional animal care and use committee.

Opto-electrophysiology setup

The opto-electrophysiology setup was developed on a Zeiss Axiovert microscope platform using an amplifier system (A-M Systems, Sequim, WA). Recordings were performed at room temperature (23–24°C). Parameters of the pipette puller were optimized to obtain the desired borosilicate micropipettes of resistance from 3 to 5 MΩ for a whole-cell patch clamp. The micropipette was filled with a solution containing (in mM) 130 K-Gluoconate, 7 KCl, 2 NaCl, 1 $MgCl_2$, 0.4 EGTA, 10 HEPES, 2 ATP-Mg, 0.3 GTP-Tris, and 20 sucrose. The electrode was mounted on a XYZ motorized micromanipulator (Eppendorf, Westbury, NY). The output from the amplifier was digitized using a National Instruments card (PCI 6221). For electrophysiological recording, the hardware was interfaced with patch-clamp software from the University of Strathclyde (Glasgow, UK; noncommercial use). The whole system was built on a vibration isolation table (Newport, Irvine, CA) and electrical isolation was done by means of an in-house-made Faraday cage that was placed around the setup. For activation of ChR2-expressing cells (identified by yellow fluorescent protein (YFP) fluorescence), a blue (473 nm, 30mW) diode laser was coupled to a 100-μm core optical fiber using a fiber coupler (Newport) mounted on a mechanical micromanipulator so as to position the tip of the fiber near the desired cell being patch-clamped. To generate and control pulses of light, the laser was interfaced with a PC. TTL pulses of desired frequency (1 Hz to a few KHz) were generated using a National Instruments (PCI 6221) card to generate the required laser pulses for activation. For electrophysiological measurements subsequent to optical activation, the diode laser source was synchronized with the patch-clamp recording electrode.

All-optical identification, activation, and detection method

To generate light activation, cells were loaded with all-trans-retinal (ATR, 1 mM) for at least 6 h and activated with a scanning laser beam. The two-photon activation of ChR2 was achieved by use of an ultrafast (fs) NIR laser (Coherent, Santa Clara, CA) microbeam (~920 nm) so as to match the single-photon absorption peak of ChR2 (~460 nm). The laser microbeam was generated by focusing the NIR beam using a microscope objective (20×, 0.5 NA). For large-area activation, the laser microbeam was scanned using a scanning device such as XY-galvanometric scanning mirrors. The average power of the scanning laser microbeam was kept below threshold level to maintain the viability of the activated cells. Further, the two-photon laser wavelength was tuned from 860 to 1028 nm to compare the relative efficiencies of the various NIR wavelengths. To visualize the activation subsequent to ChR2 activation, Ca enhancement was monitored using fluorescence (>600 nm) of a Ca indicator dye (Ca orange) with suitable excitation (543 nm). Optical detection of Ca^{2+} fluorescence subsequent to activation was carried out on a Zeiss LSM 510 META microscope. Cells without ATR incubation served as negative controls for determining any bleed-through excitation of Ca orange or YFP by the activating light beam. Cells with ATR but without YFP-ChR2 expression served as negative controls for activation.

RESULTS

Optical identification, activation, and detection

Optical detection of light-induced ChR2 activation was employed throughout the study, although patch-clamp recording was carried out to confirm (see Fig. 1 in the Supplementary Material, Data S1) light-assisted activation of ChR2-expressing cells (identified by fluorescence microscopy). This combination of optical techniques allowed us to identify, activate, and monitor excitation in multiple cells simultaneously and noninvasively. Further, we were able to activate very microscopic regions (diffraction limited spot, which contains only a few molecules of ChR2) on the membrane by single/two-photon light beams and then record Ca changes only from that confocal volume. This cannot be accomplished with patch-clamp measurements since the microscopic region of the membrane (being activated) will be damaged by the patch-clamp electrode and thus the fast changes cannot be monitored simultaneously. In Fig. 1, we show confocal laser scanning images of ChR2-YFP-expressing HEK cells (using 20× objective) and their activation process. ChR2 expression was identified by YFP imaging of HEK cells not incubated with ATR (Fig. 1 *a*) using a 514 nm Ar-ion laser beam. Changes in intracellular Ca^{2+} levels after single-/two-photon microbeam illumination were monitored using the Ca^{2+}-sensitive dye Ca orange that was excited with a 543 nm He-Ne laser beam. Fig. 1 *b* shows the basal level of fluorescence of Ca orange-stained cells without ATR, serving as a negative control. As shown in Fig. 1 *a*, though the encircled cell shows high YFP fluorescence when excited at 514 nm and detected at the 530 nm band, no bleed-through YFP fluorescence was detected (Fig. 1 *b*) in the 600 nm band (Ca orange emission band) when excited either by the 543 nm laser (used for Ca dye excitation) or by the scanning IR two-photon laser microbeam (Fig. 1 *c*). No

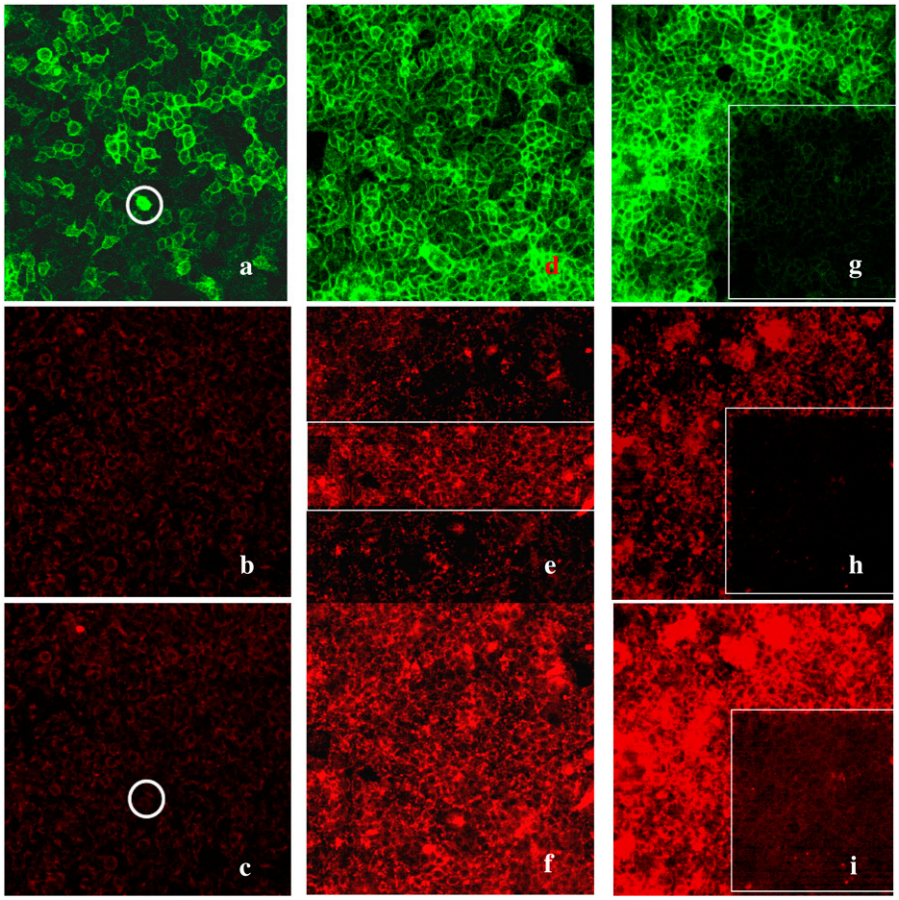

FIGURE 1 Confocal laser scanning imaging, activation, and detection of ChR2-expressing HEK cells. (*a*) ChR2 expression identified by YFP imaging (using a 20× objective) of cells not incubated with ATR. (*b*) Basal level of Ca orange fluorescence of cells without ATR. (*c*) Ca orange fluorescence subsequent to irradiation with the scanning IR two-photon laser microbeam (954 nm at power density of $\sim 1 \times 10^6$ mW/mm^2). The encircled cell shows high YFP fluorescence but no significant base level of Ca dye fluorescence (excited by 543 nm) or enhancement with the IR two-photon laser microbeam (954 nm). (*d*) YFP imaging of ChR2-expressing cells incubated with ATR. (*e*) Increase in Ca orange fluorescence subsequent to selected activation with the scanning IR two-photon laser microbeam (954 nm) in a rectangular band. (*f*) Whole-field activation with the single-photon laser microbeam (477 nm, 100 mW/mm^2). (*g*) Repeated irradiation with the NIR two-photon laser microbeam (954 nm at a power density of $\sim 1 \times 10^7$ mW/mm^2) led to damage of the cell membrane (in the rectangular region) as indicated by a decrease in YFP fluorescence as well as (*h*) basal Ca orange fluorescence. (*i*) Irradiation with the NIR two-photon laser microbeam (954 nm at a power density of $\sim 1 \times 10^6$ mW/mm^2) led to activation (indicated by increase in Ca orange fluorescence) in the intact cells.

detectable change in Ca orange fluorescence was observed (Fig. 1 *c*) subsequent to irradiation with the scanning IR two-photon laser microbeam (954 nm at power density of $\sim 1 \times 10^6$ mW/mm^2), ensuring that no bleed-through emission of Ca orange excited by the IR two-photon laser microbeam was detected in the Ca channel. Fig. 1 *d* shows YFP imaging of HEK cells incubated with ATR. An increase in Ca orange fluorescence subsequent to selected activation (in presence of ATR) with the scanning IR two-photon laser microbeam (954 nm) in a rectangular region of interest (ROI) is shown in Fig. 1 *e*. The basal level of fluorescence of Ca orange-stained cells can be seen outside the activated band in Fig. 1 *e*. Activation of ChR2-expressing cells in the whole field of view could also be achieved by a scanning laser microbeam at 477 nm (100 mW/mm^2). In Fig. 1 *f*, an increase in Ca orange fluorescence subsequent to wide-area activation with the scanning laser microbeam is observed (also see Movie S1 in the Supplementary Material, Data S1). The excitation and emission wavelengths for identification, activation, and detection are listed in Table 1. Different activation strengths (Ca fluorescence) were observed from different regions of the same cell. This inhomogeneity has several possible sources, such as nonhomogenous expression of ChR2 (as visualized by marker YFP fluorescence; Movie S2, Data S1), concentration of membrane-bound Ca indicator dye, and Ca buffering mechanisms. However, by recording from a microfocused region for all the wavelengths of activation, most of the associated variables can be removed, thus providing the activation spectrum.

Determination of threshold for repeated two-photon activation

The damage threshold for two-photon activation was determined after repeated scanning of an ROI and comparing the YFP and Ca orange fluorescence (baseline level as well as fluorescence after activation) with that of nonirradiated cells from the neighboring region. Repeated irradiation with the NIR two-photon laser microbeam (954 nm at power density of $\sim 1 \times 10^7$ mW/mm^2 scanned for 4 s with five frames per second) led to damage of the cells as noticed by a decrease in YFP fluorescence (Fig. 1 *g*). Further, baseline Ca orange

TABLE 1 Excitation and emission wavelengths for optical identification, activation, and detection

Molecule	λ_{Ex} (single photon)	λ_{Em} (detection band)
ChR2	458, 477, 488, 514 nm	—
YFP	514 nm	530 ± 10 nm
Ca orange	543 nm	600 ± 30 nm

fluorescence was also found to decrease in chronically stimulated regions (Fig. 1 *h*). However, irradiation with the NIR two-photon laser microbeam (954 nm at power density of $\sim 1 \times 10^6$ mW/mm^2) led to activation (indicated by increase in Ca orange fluorescence) in the intact cells surrounding the chronically stimulated region (Fig. 1 *i*). No significant increase in Ca orange fluorescence in the high-power chronically stimulated region further implies that the cells are not active or viable. However, no decrease in YFP or baseline Ca orange fluorescence was observed when ChR2-expressing cells were activated with the two-photon laser microbeam with an average power density below 1×10^6 mW/mm^2. Below the damage threshold, cells could be repeatedly activated with the two-photon laser microbeam, implying that cell viability was not compromised. Since the excitation spectrum of Ca orange peaks at ~543 nm, the spectral width of detection for Ca orange fluorescence and the detector gain was adjusted so as to rule out any bleed-through two-photon excitation of Ca orange and YFP even at the average power density of 1×10^6 mW/mm^2 of the laser microbeam (954 nm). Selection of YFP as an identification tag is advantageous because 1), its fluorescence wavelength is separated from Ca orange fluorescence; and 2), its two-photon excitation spectrum is narrower than other fluorescent proteins (15) and thus could be well separated from the ChR2 activation wavelength. The use of other well-separated red fluorescent proteins (mCherry) required staining with a Ca dye (e.g., Fura-2) that is excited in the UV or by a two-photon source tuned to 700 nm (data not shown).

Change in Ca fluorescence follows the single-photon ChR2 activation spectrum

To map the single-photon activation spectrum of ChR2, change in the intensity of Ca fluorescence was considered as a reliable parameter. Effects of different activation wavelengths (458, 477, 488, and 514 nm) were studied. Thresholds for detector gain and spectral width were set to minimize any bleed-through excitation of Ca orange by any of these activation wavelengths. The threshold for detectable activation (indicated by an increase in Ca orange fluorescence) was found to depend strongly on the activation wavelengths (lower for 458 nm and very high for 514 nm). For a fixed wavelength, higher power of the activating beam led to increased activation, but a saturation effect was observed thereafter. Fig. 2 *a* shows decay of Ca fluorescence by bleaching at a single excitation point (excited with 543 nm laser beam). In Fig. 2, *b–e*, we show increases in Ca orange fluorescence from a point in the plasma membrane subsequent to irradiation with visible continuous wave (cw) laser activating microbeams (focused to radius of ~0.55 μm using a 20×/0.5 NA objective). Although an increase in Ca orange fluorescence was evident on exposure to 458 nm (*b*), 477 nm (*c*), and 488 nm (*d*), at a power density of ~100 mW/ mm^2, no detectable Ca fluorescence was observed on activation with 514 nm (*e*). The red graphs in Fig. 2, *b–e*, represent scattered activation laser beams detected through a separate channel. To the best of our knowledge, this represents for the first time the activation of a microscopic region of a ChR2-expressing cell. Since the measurements were done on the same focused spot one after the other, photobleaching is observed under repeated illumination. However, this methodology of recording from the same microscopic region on the cell membrane (subsequent to different wavelength activation) was adopted to negate variabilities such as non-homogeneous distribution of ChR2 expression, membrane-bound Ca probe-dye, and Ca buffering mechanisms. The photobleaching effect was taken care of by activation with a different sequence of wavelengths at different points on the cell membrane where the same levels of initial fluorescence intensity (preactivation) were observed. The single-photon activation spectrum (Fig. 2 *f*) determined from Ca fluorescence matches published data obtained with electrophysiological recordings (16).

Mapping of the two-photon activation spectrum for ChR2

In addition to two-photon wavelengths (916, 954, 976, 1028 nm) corresponding to single-photon excitations at 458, 477, 488, and 514 nm, two other activation wavelengths (860 and 880 nm) were studied to obtain the complete two-photon activation spectrum for ChR2. Since the intensity of Ca fluorescence was considered as a detection parameter for ChR2 activation, thresholds for detector gain and spectral band were set to minimize any bleed-through excitation of Ca orange by any of these two-photon activation wavelengths. Although detectable activation at 916 nm was observed at very low power densities, 1028 nm activation required considerably higher power levels for similar activation (Ca orange fluorescence). When a 100-ms train of NIR fs pulses (916 nm; 97.64 MHz) was focused on the ChR2-expressing cell membrane, the Ca orange fluorescence increased instantaneously and decayed within <0.1 s of the NIR fs pulse train (Fig. 2 in the Supplementary Material, Data S1). This implies that stimulation of up to 10 Hz can be detected by changes in Ca orange fluorescence. The use of fast Ca indicator probes (17) and imaging systems (18) can allow even faster optical detection subsequent to optical activation over a wide sample. Steady illumination with NIR fs pulses (97.64 MHz) evoked a single reliably timed spike, followed by irregular spiking. In Fig. 3 we show an increase in Ca orange fluorescence subsequent to NIR fs laser microbeam irradiation (focused to radius of ~1.1 μm using a 20× objective). On exposure to an 860 nm laser microbeam, a very small change in Ca orange fluorescence (excited with a 543 nm laser beam at the same point) from a point in the plasma membrane was observed (Fig. 3 *a*). Ca orange fluorescence was observed to increase more after exposure to 916 nm (*c*) than after exposure to 880

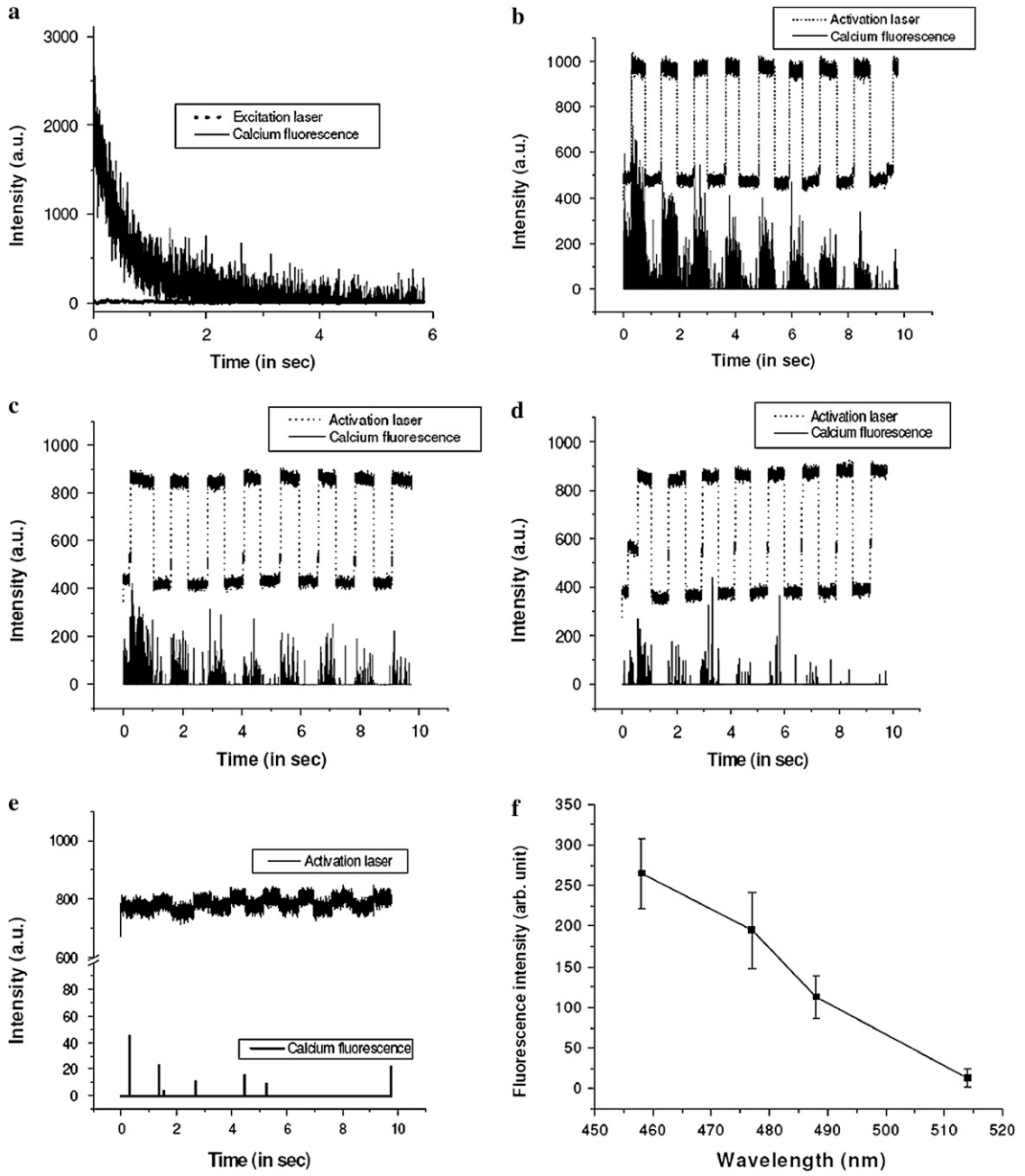

FIGURE 2 Single-photon activation spectrum determined by mapping increase in Ca orange fluorescence (excited with a 543 nm laser beam at the same point) subsequent to irradiation with a visible cw laser activating the microbeam (focused to a radius of ~0.55 μm using a 20× objective). (*a*) Decay of Ca fluorescence by bleaching at a single excitation point. (*b*) Change in Ca orange fluorescence from a point in the plasma membrane on exposure to 458 nm, (*c*) 477 nm, and (*d*) 488 nm. (*e*) No detectable Ca fluorescence was observed on activation with 514 nm. In *a*, the red graph represents the fluorescence excitation beam (543 nm), and in *b–e* it represents scattered activation laser beams detected through a separate channel. (*f*) Single-photon activation spectrum obtained from measurements over 25 points on five different cells. The power density of the activating laser beam was kept at ~100 mW/mm^2.

nm (*b*). Increasing the activation wavelength to 954 nm and 976 nm at the same average power density of $\sim 1.0 \times 10^6$ mW/ mm^2, Ca orange fluorescence was found again to decrease (*d* and *e*). Corresponding to the one-photon activation at 514 nm (Fig. 2 *e*), two-photon activation using 1028 nm led to a minimal increase in Ca fluorescence (*e*) similar to levels obtained with 860 nm activation (*a*). Thus, for the first time we were able to map a two-photon activation spectrum of ChR2 (*g*). Though the average two-photon power density required to elicit similar activation effects was found to be higher as compared to that for single-photon activation, selected activation with high spatial resolution in three dimensions is better achievable with two-photon activation since the two-photon process requires

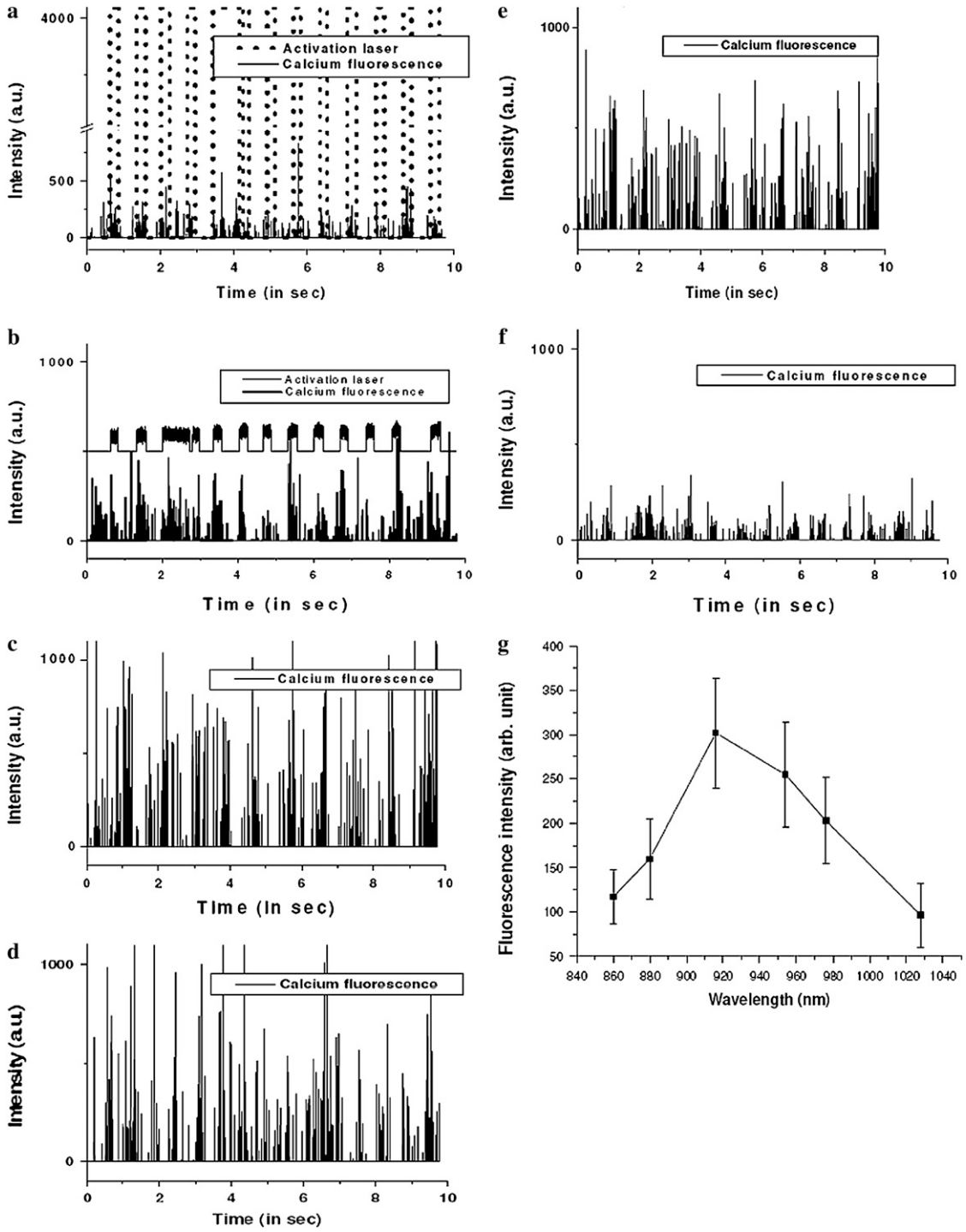

FIGURE 3 Mapping increase in Ca orange fluorescence subsequent to NIR fs laser microbeam irradiation (focused to a radius of ~1.1 μm using a 20× objective). (*a*) Very small change in Ca orange fluorescence (excited with 543 nm laser beam at the same point) from a point in the plasma membrane, on exposure to the 860 nm laser microbeam. Increasing change in Ca orange fluorescence observed on exposure to (*b*) 880 nm and (*c*) 916 nm. Ca orange fluorescence was found to decrease on exposure to (*d*) 954 nm and (*e*) 976 nm, and is almost undetectable at 1028 nm (*f*). The average power density of the activating laser beam was kept at $\sim 1.0 \times 10^6$ mW/ mm^2. The red graphs in *a* and *b* represent scattered activation laser beams detected through a separate channel. In *c–f*, the pulses of scattered activation at longer wavelengths could not be detected due to technical limitations. (*g*) Two-photon activation spectrum determined from measurements over 30 points on six different cells.

high peak power, which happens only in a very small three-dimensional volume.

Dose dependence of the two-photon activation shows nonlinearity

Similarly to single-photon activation for a fixed wavelength, higher power of the activating beam led to increased activation. Fig. 4 shows the dependence of Ca orange fluorescence (excited with a 543 nm laser beam at the same point on the plasma membrane) on the power density of the two-photon laser microbeam (916 nm, focused to a radius of ~1.1 μm using a 20× objective). Fluorescence intensity (as a measure of activation) is found to increase in a nonlinear manner (*e*) with the power density of the two-photon laser microbeam from 3.9×10^5 to 15.6×10^5 mW/mm^2. However, when the power density was increased beyond 15.6×10^5 mW/mm^2, saturation of fluorescence intensity was noticed. This can be attributed to two facts: 1), the number of ChR2 molecules to be activated in the focused spot (radius of ~1.1 μm) is exhausted; and 2), Ca orange fluorescence is known to increase only threefold at the maximum (19). The second effect can be ruled out by the use of suitable probes having larger dynamic ranges for measuring changes of intracellular Ca. However, care should be taken to ensure that the excitation spectrum of the Ca indicator dye does not overlap with that of ChR2 and the fluorescent protein used to identify the expression of ChR2 (see Fig. 3 in the

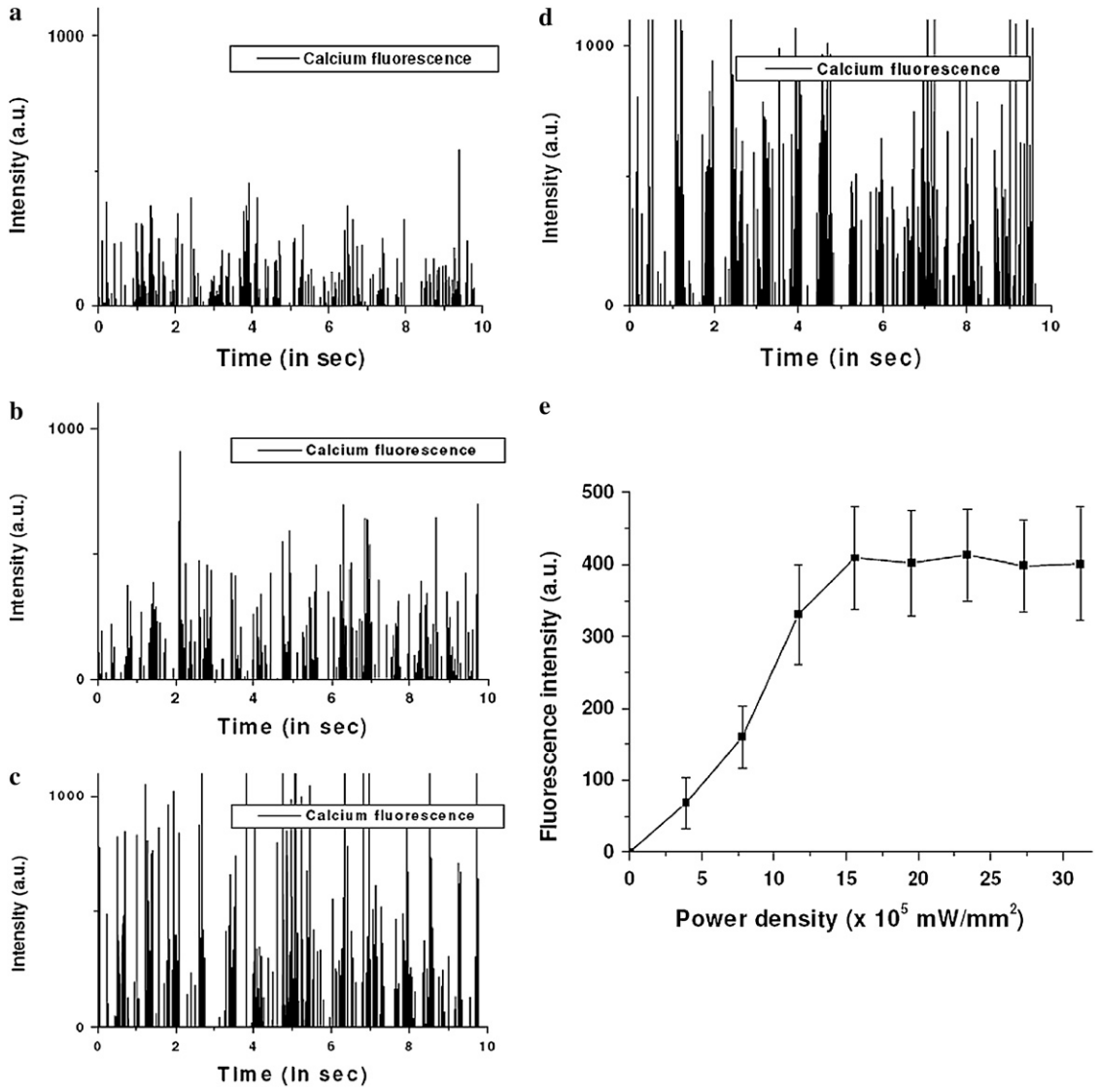

FIGURE 4 Dependence of Ca orange fluorescence (excited with a 543 nm laser beam at the same point on the plasma membrane) on the power density of the two-photon laser microbeam (916 nm, focused to a radius of ~1.1 μm using a 20× objective): (*a*) 3.9×10^5, (*b*) 7.8×10^5, (*c*) 11.7×10^5, and (*d*) 15.6×10^5 mW/mm^2. (*e*) Fluorescence intensity (as a measure of activation) as a function of power density of the two-photon laser microbeam, determined from measurements over 20 points on four different cells. The pulses of scattered activation at longer wavelengths could not be detected due to technical limitations.

Supplementary Material, Data S1). Beyond a power density of $\sim 0.5 \times 10^7$ mW/mm^2, for short exposure (0.1 s), Ca influx was seen to increase and remain steady for quite long periods (Fig. 4 in the Supplementary Material, Data S1). This can be attributed to the fact that at this power density, optoporation (12) of extracellular Ca can occur. This was confirmed by varying the wavelength of the fs laser microbeam over the whole range from 860 to 1028 nm. As expected, optoporation (as measured by an increase in Ca orange fluorescence) was found to depend on the power density and to be independent of the wavelength of the laser beam.

Two-photon activation leads to better in-depth activation efficacy

Most of the studies reported in the past were based on exciting cells near the superficial layers in close proximity to the blue light source (4–9). Since the blue light is absorbed and scattered significantly by the cells or biological tissues, this method will not be suitable for activating cells at larger depths, as required for in vivo applications. Cells at larger depths can only be reached by increasing the average power of the single-photon light beam, which will lead to significant detrimental effects on the viability of cells closer to the single-photon source. However, scanning two-photon light of relatively low average power (a few milliwatts) in the NIR region can penetrate deeper into the tissue and thus would be more effective in achieving the activation process. In Fig. 5 we show a comparison of in-depth activation efficacy (measured as the maximum depth where Ca orange fluorescence is detected) of ChR2-expressing neuronal cells in mouse hippocampus. ChR2-expression was confirmed by YFP imaging as shown in Fig. 5 *a*. The basal level of Ca orange fluorescence at depths of 180 (*b*), 200 (*c*), 220 (*d*), and 240 μm (*e*) was detected with 543 nm excitation. Single-photon activation (*f–j*: 458 nm; *k–o*: 477 nm) with the laser microbeam (1.0×10^3 mW/mm^2) led to an increase in Ca orange fluorescence at all depths investigated (160–240 μm in intervals of 20 μm). For comparison with two-photon activation, the intensity of the NIR fs laser microbeam (916 nm) was adjusted to achieve activation (*p*) similar to that of the single-photon laser source at a depth of 160 μm. Fig. 5, *p–t,* shows an increase in Ca orange fluorescence due to two-photon irradiation at various depths. Histograms of Ca orange fluorescence versus wavelength of activation at depths of 160 (*u*) and 180 μm (*v*) show equivalent activation intensity for 458, 477, and 916 nm. However, at increasing depths (*w–y*), higher activation due to the two-photon NIR microbeam was observed as compared to single-photon excitation. Similar results were observed in a spheroid model of HEK cells expressing ChR2-EYFP (see Fig. 5 in the Supplementary Material, Data S1). It may be noted that the depth of our measurements is also limited by the penetration depth of the excitation wavelength (543 nm) of Ca orange, and therefore a two-photon source can be used for activation and Ca imaging as well. However, this would require either fast switching between two wavelengths (e.g., ~900 nm for activation and ~1100 nm for imaging in our case) or the use of two separate two-photon sources.

DISCUSSION

This study presents an all-optical method to simultaneously detect, excite, and monitor cellular activity in cells expressing the light-activated cation channel ChR2. Furthermore, by using two-photon activation with NIR light, enhanced tissue penetration with reduced photodamage was achieved, which will benefit future in vivo applications of this technology. Previous approaches have used combinations of optical and electrophysiological methods that posed severe limitations for in vivo use. For example, simultaneous electrophysiological recording from multiple light-activated cells is virtually impossible. Detection of electrical signals from every single ChR2-expressing cell would require electrodes implanted inside every cell, making even in vitro detection from a tissue slice not feasible. Electrodes have limited spatial resolution, and because electrode methodologies rely on mechanical stability, they are cumbersome to use. In contrast, with the use of optical detection methods, large numbers of cells can be studied simultaneously. With optical detection, the whole process of identification, activation, and quantification of intracellular biochemical events is noninvasive and has the added advantages of high throughput, no contamination, and the least requirement of mechanical stability as encountered for electrical activation/detection.

Although genetic targeting of cells or tissues with light-activated proteins allows for simultaneous activation of a defined cell population, some experiments may necessitate selective activation of single cells or even different regions within the same cell. Since the two-photon process is nonlinear in nature, NIR activation will have definite advantages over single-photon methods in highly localized activation of the specific cell in a cluster or even a small ROI of a single cell. The two-photon activation method presented here will also enable penetration up to a few millimeters into biological tissues and thus effectively activate specific ChR2-expressing cells in in vivo conditions. In contrast, while using single-photon activation (even at 473 nm), more than 99% of the incident intensity is lost at a depth of 1 mm in cortical tissue (20). Although 90% of the incident power is lost because of the optical properties of the tissue, divergence of the beam from the fiber accounts for additional loss. The divergence can be eliminated by the use of an axicon tipped fiber (21) to generate nondiffracting Bessel beams; for in vivo use, fiber endoscopes (22,23) can be designed to achieve two-photon activation over desired regions. Further, the same two-photon activation source can be tuned to optically image the ChR2-coupled fluorescent protein expressing cells and also to monitor Ca changes generated subsequent to ChR2 activation by use of suitable Ca indicator dyes. This will

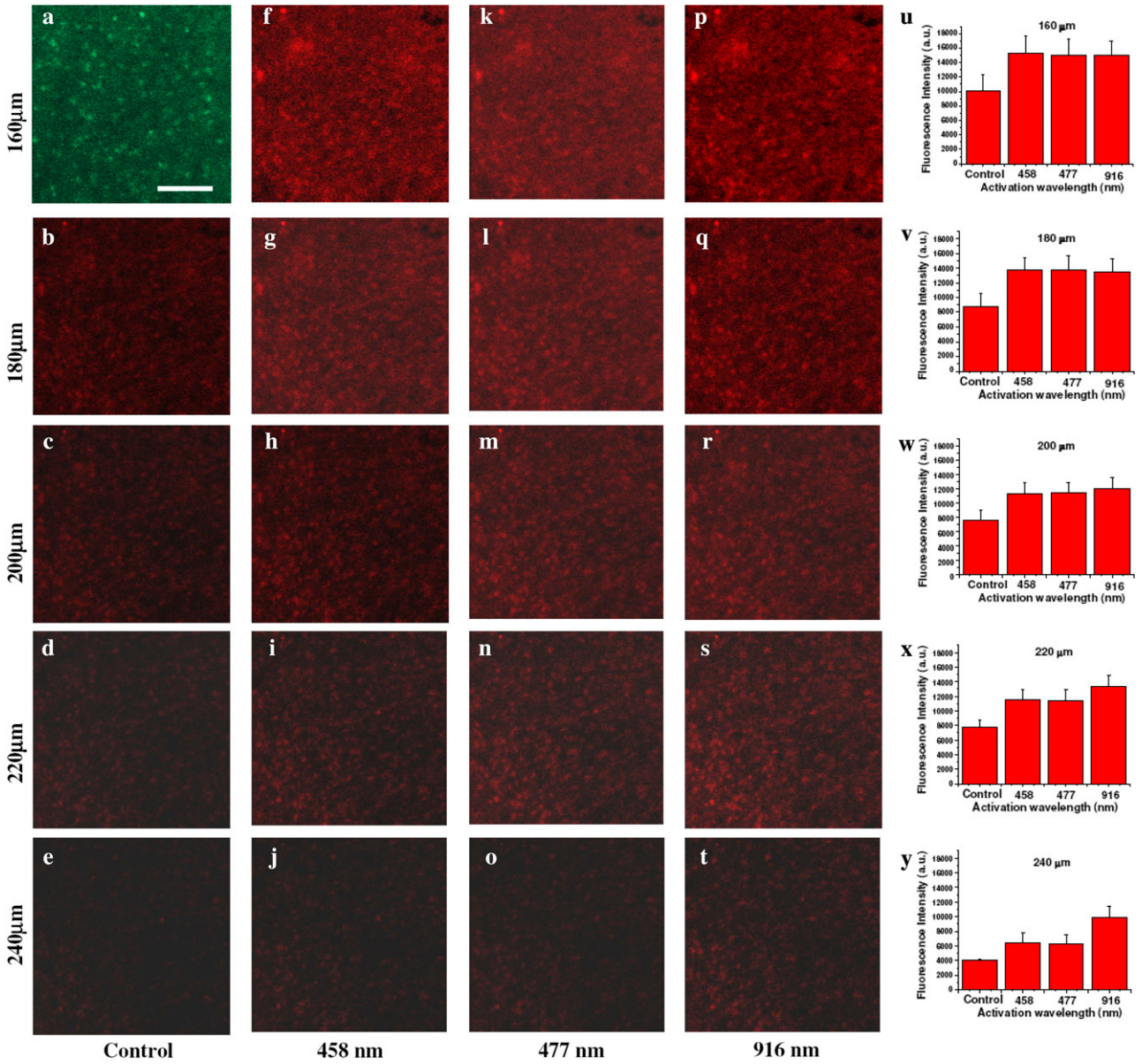

FIGURE 5 Comparison of in-depth activation efficacy (measured by the maximum depth from which Ca orange fluorescence is detected) of ChR2-expressing neuronal cells in mouse hippocampus. (*a*) ChR2-expression observed by YFP imaging. (*b–e*) Basal level of Ca orange fluorescence at depths of 180, 200, 220, and 240 μm, respectively. (*f–j*) Single-photon activation with a laser microbeam (458 nm, 1.0×10^3 mW/mm^2). (*k–o*) Activation with 477 nm. (*p–t*) Two-photon irradiation with the NIR laser microbeam (916 nm) leading to an increase in Ca orange fluorescence at all depths. Histogram of fluorescence intensity (as a measure of activation efficiency) versus wavelength of activation at depths of 160 μm (*u*), 180 μm (*v*), 200 μm (*w*), 220 μm (*x*), and 240 μm (*y*). Scale bar in *a* represents 200 μm.

eliminate the need to implant patch-clamping electrodes, which are generally employed to record the activation process. These added advantages of two-photon optical activation and imaging will help us to better understand and modulate the physiological functions of various excitable cells in skeletal, cardiac, and neuronal systems, and also accelerate high-throughput ion-channel drug screening. With the invention of other light-activated channels, such as NpHR (24), in which the peak of the action spectrum is in the visible wavelength range, the present two-photon method can also be used to achieve in-depth inhibition of cellular activity with high spatial and temporal precision.

In the experiments presented in this study, two-photon activated signals are observed at greater depths when compared to attenuated single-photon activation (as shown in Fig. 5). However, the Ca orange signals, in response to two-photon activation recorded from a point volume (diffraction limited spot radius ~1.1 μm) on monolayer cell membranes, are weaker (Fig. 3) than the single-photon

activated signals. This may be attributed to the fact that a smaller three-dimensional volume is activated with the two-photon source as compared to the single-photon beam, and also to the low two-photon cross section of ChR2. It may be noted that ChR2 has so far been heterologously expressed only in small amounts, and no protein is available for spectroscopic studies. When enough ChR2 protein becomes available, spectroscopic measurements on ChR2 will certainly enable measurement of the two-photon cross section. The following simplified calculations may help to explain the observations mentioned above: To estimate the number of ChR2 molecules in the activated microscopic area, we assume an expression density of ChR2 in the plasma membrane similar to BR (25) (i.e., 130 per μm^2). So, in our case, a focused area of ($\sim$3.8 μm^2) will contain $\sim$34 ChR2 molecules. Assuming that only a small percentage of ChR2 are in the open state (see the model on the photocycle in Nagel et al. (5)), only a few ChR2 molecular channels will allow Ca to influx into the focused spot. This would lead to a decrease in Ca fluorescence signal recorded from microscopic spots subsequent to single-/two-photon activation, and would explain the requirement of high-power density as compared to lower-power density in simultaneous wide-field illumination.

Two-photon irradiation reduces specimen photodamage by localizing the excitation region to very small volumes. Further, the damage threshold increases by several orders of magnitude when using an infrared microbeam (26) as compared to UV/visible radiation. Although long-term monitoring of embryos of *C. elegans* and hamster using single-photon confocal microscopy failed because of photodamage-induced developmental arrest, two-photon microscopy (27) did not cause observable damage. Hence, two-photon microscopy is finding widespread applications for in vivo measurement of physiological functions (28–31). However, femtosecond NIR microirradiation above certain threshold power levels has been shown to affect cell vitality and cellular reproduction (32). This is consistent with the observed photodamage (described here) induced by two-photon activation of ChR2-expressing cells at higher average power levels. More studies are under way to elucidate the mechanisms of damage in two-photon activated ChR2-expressing cells.

CONCLUSIONS

The presented all-optical method for imaging and simultaneous activation of ChR2 and subsequent Ca imaging of large populations of selected excitable cells will not only lead to a better understanding of basic biological phenomena, it will also accelerate ion-channel drug discovery, which is presently achieved by patch-clamp methods in electrophysiology. Two-photon activation allowed activation at greater depths, as required for in vivo applications, and also provided the high spatial resolution that is necessary for experiments requiring single-cell or region-specific excitation.

SUPPLEMENTARY MATERIAL

To view all of the supplemental files associated with this article, visit www.biophysj.org.

We acknowledge a Material Transfer Agreement for the ChR2 cDNA construct, obtained from Dr. Georg Nagel, Max Planck Institute for Biophysics, Frankfurt, Germany, signed and executed November 7, 2006. We thank Joanne Zeng for expert technical assistance with cell culture, and Dr. R. Meyer for access to the vibratome. This research was supported in part by grants from the U.S. Air Force (grant AFOSR), the Beckman Laser Institute (to M.W.B.), and the Laser Microbeam and Medical Program (LAMMP, P41RR01192).

S. K. M., M. W. B., and R. K. R. designed the research. S. K. M. performed the experiments and wrote the article. X. L. generated the ChR2-EYFP construct, established transfected cells, and prepared lentiviral vectors. N. O. and R. K. R. performed viral injections in mouse brain and subsequent histological preparations. T. K. maintained the Zeiss LSM 510 META microscope.

REFERENCES

1. Ehrlicher, A., T. Betz, B. Stuhrmann, D. Koch, V. Milner, M. G. Raizen, and J. Kas. 2002. Guiding neuronal growth with light. *Proc. Natl. Acad. Sci. USA.* 99:16024–16028.
2. Hirase, H., V. Nikolenko, J. H. Goldberg, and R. Yuste. 2002. Multiphoton stimulation of neurons. *J. Neurobiol.* 51:237–247.
3. Mohanty, S. K., M. Sharma, M. Panicker, and P. K. Gupta. 2005. Controlled induction, enhancement, and guidance of neuronal growth cones using line optical tweezers. *Opt. Lett.* 30:2596–2598.
4. Miller, G. 2006. Shining new light on neural circuits. *Science.* 314: 1674–1676.
5. Nagel, G., T. Szellas, W. Huhn, S. Kateriya, N. Adeishvili, P. Berthold, D. Ollig, P. Hegemann, and E. Bamberg. 2003. Channelrhodopsin-2, a directly light-gated cation-selective membrane channel. *Proc. Natl. Acad. Sci. USA.* 100:13940–13945.
6. Zhang, F., L. Wang, E. S. Boyden, and K. Deisseroth. 2006. Channelrhodopsin-2 and optical control of excitable cells. *Nat. Methods.* 3:785–792.
7. Boyden, E. S., F. Zhang, E. Bamberg, G. Nagel, and K. Deisseroth. 2005. Millisecond-timescale, genetically targeted optical control of neural activity. *Nat. Neurosci.* 8:1263–1268.
8. Nagel, G., M. Brauner, J. F. Liewald, N. Adeishvili, E. Bamberg, A. Gottschalk. 2005. Light activation of channelrhodopsin-2 in excitable cells of *Caenorhabditis elegans* triggers rapid behavioral responses. *Curr. Biol.* 15:2279–2284.
9. Schroll, C., T. Riemensperger, D. Bucher, J. Ehmer, T. Völler, K. Erbguth, B. Gerber, T. Hendel, G. Nagel, E. Buchner, A. Fiala. 2006. Light-induced activation of distinct modulatory neurons triggers appetitive or aversive learning in Drosophila larvae. *Curr. Biol.* 16:1741–1747.
10. Parrish, A. R., W. Wang, and L. Wang. 2006. Manipulating proteins for neuroscience. *Curr. Opin. Neurobiol.* 16:585–592.
11. Denk, W., J. H. Strickler, and W. W. Webb. 1990. Two-photon laser scanning fluorescence microscopy. *Science.* 248:73–76.
12. Tirlapur, U. K., and K. Konig. 2002. Targeted transfection by femtosecond laser. *Nature.* 418:290–291.
13. Berns, M. W., Z. Wang, A. Dunn, V. Wallace, and V. Venugopalan. 2000. Gene inactivation by multiphotontargeted photochemistry. *Proc. Natl. Acad. Sci. USA.* 97:9504–9507.
14. Zhang, Y., and T. G. Oertner. 2007. Optical induction of synaptic plasticity using a light-sensitive channel. *Nat. Methods.* 4:139–141.
15. Blab, G. A., P. H. M. Lommerse, G. S. H. Cognet, and T. Schmidt. 2001. Two-photon excitation action cross-sections of the autofluorescent proteins. *Chem. Phys. Lett.* 350:71–77.

16. Zhang, F., A. M. Aravanis, A. Adamantidis, L. Lecea, and K. Deisseroth. 2007. Circuit-breakers: optical technologies for probing neural signals and systems. *Natl. Rev.* 8:577–581.

17. Tour, O., S. R. Adams, R. A. Kerr, R. M. Meijer, T. J. Sejnowski, R. W. Tsien, R. Y. Tsien. 2007. Calcium Green FlAsH as a genetically targeted small-molecule calcium indicator. *Nat. Chem. Biol.* 3:423–431.

18. Demuro, A., and I. Parker. 2005. Optical patch-clamping: single-channel recording by imaging Ca^{2+} flux through individual muscle acetylcholine receptor channels. *J. Gen. Physiol.* 126:179–192.

19. Eberhard, M., and P. Erne. 1991. Calcium binding to fluorescent calcium indicators: calcium green, calcium orange and calcium crimson. *Biochem. Biophys. Res. Commun.* 180:209–215.

20. Aravanis, A. M., L. P. Wang, F. Zhang, L. A. Meltzer, M. Z. Mogri, M. B. Schneider, K. Deisseroth. 2007. An optical neural inteface: *in vivo* control of rodent motor cortex with integrated fiberoptic and optogenetic technology. *J. Neural Eng.* 4:S143–S156.

21. Verma, Y., K. D. Rao, S. K. Mohanty, and P. K. Gupta. 2007. Tapered single mode fiber tip high lateral resolution optical coherence tomography. *Laser Phys. Lett.* 4:686–689.

22. Bird, D., and M. Gu. 2003. Two-photon fluorescence endoscopy with a micro-optic scanning head. *Opt. Lett.* 28:1552–1554.

23. Jung, J. C., and M. J. Schnitzer. 2003. Multiphoton endoscopy. *Opt. Lett.* 28:902–904.

24. Zhang, F., L. Wang, M. Brauner, J. F. Liewald, K. Kay, N. Watzke, P. G. Wood, E. Bamberg, G. Nagel, A. Gottschalk, and K. Deisseroth. 2007. Multimodal fast optical interrogation of neural circuitry. *Nature.* 446:633–639.

25. Nagel, G., B. Mockel, G. Buldt, and E. Bamberg. 1995. Functional expression of bacteriorhodopsin in oocytes allows direct measurement of voltage dependence of light induced H^+ pumping. *FEBS Lett.* 377:263–266.

26. Mohanty, S. K., A. Rapp, S. Monajembashi, P. K. Gupta, and K. O. Greulich. 2002. COMET assay measurement of DNA damage in cells by laser microbeams and trapping beams with wavelengths spanning a range of 308 nm to 1064 nm. *Radiat. Res.* 157:378–385.

27. Squirrell, J. M., D. L. Wokosin, J. G. White, and B. D. Bavister. 1999. Long-term two-photon Fluorescence imaging of mammalian embryos without compromising viability. *Nat. Biotechnol.* 17:763–767.

28. Brown, E. B., R. B. Campbell, Y. Tsuzuki, L. Xu, P. Carmeliet, D. Fukumura, R. K. Jain. 2001. In vivo measurement of gene expression, angiogenesis and physiological function in tumors using multiphoton laser scanning microscopy. *Nat. Med.* 7:864–868.

29. Stosiek, C., O. Garaschuk, K. Holthoff, and A. Konnerth. 2003. *In vivo* two-photon calcium imaging of neuronal networks. *Proc. Natl. Acad. Sci. USA.* 100:7319–7324.

30. Zipfel, W. R., R. M. Williams, and W. W. Webb. 2003. Nonlinear magic: multiphoton microscopy in the biosciences. *Nat. Biotechnol.* 21:1369–1377.

31. Helmchen, F., and W. Denk. 2005. Deep tissue two-photon microscopy. *Nat. Methods.* 2:932–940.

32. Konig, K., P. T. C. So, W. W. Mantulin, and E. Gratton. 1997. Cellular response to near-infrared femtosecond laser pulses in two-photon microscopes. *Opt. Lett.* 22:135–136.